

Schwinger Pair Production in QCD from Flavor-Dependent Contact Interaction Model of Quarks

Aftab Ahmad, Akif Farooq

Institute of Physics, Gomal University, 29220, D.I. Khan, Khyber Pakhtunkhaw, Pakistan.

E-mail: aftabahmad@gu.edu.pk, akiffarooq143@gmail.com

Abstract. We study the Schwinger mechanism in QCD i.e., the quark-antiquark pair production rate Γ in the presence of pure electric field strength eE , for a higher number of colors N_c and flavors N_f . In this context, our unified formalism is based on the Schwinger-Dyson equations, flavor-dependent symmetry preserving vector-vector contact interaction model of quarks, and an optimal time regularization scheme. For fixed $N_c = 3$ and $N_f = 2$, the dynamically quark mass decreases as we increase eE and near at and above the pseudo-critical electric field eE_c , the chiral symmetry is restored and quarks becomes unconfined. The pair production rate Γ becomes stable and grows quickly above eE_c . For fixed $N_c = 3$ and upon increasing N_f the dynamical mass suppresses and as a result, the eE_c reduces to its smaller values, the pair production rate Γ tends to initiates and grows quickly for smaller values of eE_c . In contrast, for fixed $N_f = 2$ and upon increasing N_c , the dynamical chiral symmetry is restored for larger and larger values of eE_c and at $N_c \geq 4$, the transition changes from smooth cross-over to the first order at some critical endpoint $(N_{c,p}, eE_{c,p})$. Consequently, the quark-antiquark production rate Γ needs higher values of eE_c for the stable and quick growth as we increase N_c . Our findings are satisfactory and in agreement with already predicted results for pair production rate (for fixed $N_c = 3$ and $N_f = 2$) by other reliable effective models of QCD.

Keywords: Chiral symmetry breaking, confinement, electric field, Schwinger-Dyson equations, QCD phase diagram

1. Introduction

Historically, the phenomenon of electron-positron pair production from a non-perturbative vacuum in the presence of electric field strength eE (where e is an electric charge) was first introduced by Fritz Sauter [1], Heisenberg and Euler [2]. However, the complete theoretical framework provided by Julian Schwinger in the field of quantum electrodynamics (QED) [3], and named after him as the Schwinger effect or Schwinger mechanism. Later on, this phenomenon has been widely studied in the field of quantum chromodynamics (QCD), see for example, Refs. [4, 5, 6, 7, 8]. As we know that the QCD is a theory of strong color force among the quarks and gluons possess two special properties: The asymptotic freedom (i.e., the quarks interacts weakly at a short distances or high energy scale) and the quark confinement (i.e., the quarks interacts strongly at a large distance or low energy scale). The Schwinger effect in QCD is thus, the production of quark-antiquark pairs in the presence of a strong electric field eE . The quark-antiquark pair production can be calculated from the Schwinger pair production rate Γ and is, defined as the probability, per unit time and per unit volume that a quark-antiquark pair is created by the constant electric field eE .

Another important property of low-energy QCD is the dynamical chiral symmetry breaking, which is related to the dynamical mass generation of the quarks. The strong electric field tends to restore the dynamical chiral symmetry and as a result, the dynamically generated quark mass suppresses with the increase of eE . It can be understood by realizing that being closer together, the quark and antiquark pairs are reaching the asymptotic freedom regime faster by reducing the interaction strength as the intensity of the electric field eE increases. Such a phenomenon is sometimes referred to as the chiral electric inhibition effect [9, 6, 10, 11, 12, 13, 14], or the chiral electric rotation effect [15] or inverse electric catalysis(IEC) [16, 17, 18]. The nature of the dynamical chiral symmetry breaking–restoration and confinement–deconfinement phase transition is of second-order when the bare quark mass $m = 0$ (i.e., in the chiral limit) while cross-over when $m \neq 0$. It has been argued in Refs. [13, 14, 17] that the pair production rate Γ , increases quickly near some pseudo-critical electric field eE_c , where the chiral symmetry is restored.

The study of the effect of the electric field on the chiral phase transition plays a significant role in Heavy-Ion Collision experiments. In such experiments, the magnitude of the electric and magnetic fields produced with the same order of magnitude ($\sim 10^{18}$ to 10^{20} Gauss) [19, 20, 21, 22] in the event-by-event collisions using Au + Au at RHIC-BNL, and in a non-central Heavy-Ion collision of Pb + Pb in ALICE-LHC. Besides, experiments with asymmetric Cu + Au collisions, it is believed that the strong electric field is supposed to be created in the overlapping region [23, 24, 25]. It happens because there are different numbers of electric charges in each nuclei, which may be due to the charge dipole formed in the early stage of the collision. Some other phenomena like the chiral electric separation effect [26, 27], the particle polarization effect [28, 29, 30], etc., which may emerge due to the generation of vector and/or axial current in the presence

of strong electromagnetic fields.

It is illustrative to approximate the created number of charged quark-antiquark pairs in the QGP produces in Heavy Ion collision, because in the QGP phase the dynamical chiral symmetry restores and the deconfinement occurs. According to advance numerical simulations, the electric fields created in Au + Au collisions at center-of-mass energy $\sqrt{s} = 200$ GeV due to the fluctuation is of the order $eE \sim m_\pi^2$ while in Pb+Pb collisions at $\sqrt{s} = 2.76$ TeV is of the order $eE \sim 20m_\pi^2$ [20]. Then by assuming the space-time volume of the QGP is of the order $\sim (5\text{fm})^4$, the total pair creation number is $N_{\text{RHIC}} = 3.5$, and $N_{\text{LHC}} = 1400$ [31], gives us a clear indication of the importance of Schwinger pair production of quark and antiquark in Heavy Ion Collisions.

It is well understood that the QCD exhibits confinement and chiral symmetry breaking with the small number of light quark flavors N_f . However, for larger N_f , Lattice QCD simulation [32, 33, 34, 35, 36], as well as the continuum methods of QCD [37, 38, 39, 40, 41, 42, 18, 43], predicted that there is a critical value $N_f^c \approx 8$ above which the chiral symmetry is restored and quarks become unconfined. It has been discussed in detail in Ref. [18] that the critical number of flavors N_f^c suppresses with the increase of temperature T and enhances with the increasing magnetic field eB . Even the QCD phase diagram at finite temperature T and density μ suppresses with the increase of light quark flavors, see for an instance Ref. [42]. Besides the higher number of light quark flavors, QCD with a larger number of colors N_c in the fundamental $SU(N_c)$ representation also plays a significant role. It has been demonstrated in Ref. [18, 42] that the chiral symmetry is dynamically broken above a critical value $N_c^c \approx 2.2$, as a result, the dynamically generated mass increases near and above N_c^c . Increasing the number of colors also enhances the critical temperature T_c and the critical chemical potential μ_c of the chiral phase transition in the QCD phase diagram [18]. Both N_c and magnetic field eB strengthen the generation of the dynamical masses of the quarks [42].

It will be more significant to study the dynamical chiral symmetry breaking and Schwinger effect in pure electric field background for a higher number of light quark flavors N_f and for a large number of colors N_c , which has not yet been studied so far, as far as we know. It may have a stronger impact not only on the theoretical ground but also in Heavy-Ion Collision experiments where a large number of light flavors of quark-antiquark pairs are produced. Our main objective of this work is to study the quark-antiquark pair production rate in the presence of a pure electric field eE background for a higher number of light quark flavors N_f and colors N_c . For this purpose, we use the Schwinger-Dyson equation in the rainbow-ladder truncation, in the Landau gauge, the symmetry preserving flavour-dependent confining vector-vector contact interaction model of quarks [18], and the Schwinger optimal time regularization scheme [3]. The pseudo-critical electrical field strength eE_c , the critical number of flavors N_f^c and the critical number of colors N_c^c for chiral symmetry breaking-restoration can be obtained from the peak of the correspondence gradient of dynamical quark mass, whereas the confinement-deconfinement can be triggered from the peaks of correspondence gradient

of the confining length scale [44, 18, 42]. It should be noted that the chiral symmetry restoration and deconfinement occur simultaneously in this model [45, 44, 18, 42].

This manuscript is organized as follows: In Sec. 2, we present the general formalism for the flavor-dependent contact interaction model and QCD gap equation. In Sec. 3, We discuss the gap equation and the the Schwinger pair production rate in the presence of electric field eE for a large number of flavors N_f and colors N_c . In Sec. 4, we present the numerical solution of the gap equation and the Schwinger pair production rate in the presence of eE for a higher number of N_f and N_c . In the last Sec. 5, we present the summary and future perspective of our work.

2. General formalism and flavor-dependent Contact Interaction model

The Schwinger-Dyson equations (SDE) for the dressed-quark propagator S , is given by:

$$S^{-1}(p) = S_0^{-1}(p) + \Sigma(p), \quad (1)$$

where $S_0(p) = (\not{p} + m + i\epsilon)^{-1}$, is the bare quark propagator and $S(p) = (\not{p} + M + i\epsilon)^{-1}$ is the dressed quark propagator. The $\Sigma(p)$ is the self energy and is given by

$$\Sigma(p) = \int \frac{d^4k}{(2\pi)^4} g^2 D_{\mu\nu}(q) \frac{\lambda^a}{2} \gamma_\mu S(k) \frac{\lambda^a}{2} \Gamma_\nu(p, k), \quad (2)$$

where $\Gamma_\nu(k, p)$ is the dressed quark-gluon vertex and g^2 is the QCD coupling constant. The $D_{\mu\nu}(q) = D(q)(\delta_{\mu\nu} - \frac{q_\mu q_\nu}{q^2})$ is the gluon propagator in the Landau gauge with $\delta_{\mu\nu}$ is the metric tensor in Euclidean space, $D(q)$ is the gluon scalar function and $q = k - p$ is the gluon four momentum. The m is the current quark mass, which may set equal to zero (i.e., $m = 0$) in the chiral limit. The λ^a 's are the Gell-Mann matrices and in the $SU(N_c)$ representation, the Gell-Mann's matrices satisfies the following identity:

$$\sum_{a=1}^8 \frac{\lambda^a}{2} \frac{\lambda^a}{2} = \frac{1}{2} \left(N_c - \frac{1}{N_c} \right) I, \quad (3)$$

here I is the unit matrix. In this work, we use the symmetry preserving flavor-dependent confining contact interaction model [42, 43] for the gluon propagator (in Landau gauge) in the infrared region where the gluons dynamically acquire a mass m_g [46, 47, 48, 49, 50], is given by

$$g^2 D_{\mu\nu}(k) = \frac{4\pi\alpha_{\text{ir}}}{m_G^2} \sqrt{1 - \frac{(N_f - 2)}{\mathcal{N}_f^c}} \delta_{\mu\nu} = \delta_{\mu\nu} \alpha_{\text{eff}} \sqrt{1 - \frac{(N_f - 2)}{\mathcal{N}_f^c}}, \quad (4)$$

the $\alpha_{\text{ir}} = 0.93\pi$ is the infrared enhanced interaction strength parameter, $m_g = 800$ MeV is the gluon mass scale [51]. The $\mathcal{N}_f^c = N_f^c + \eta$ is some guess values of critical number of flavors. In Ref. [42, 43], the value of η has been set and it ranging from 1.8 – 2.3, to obtained the desired number of critical number $N_f^c \approx 8$ above which the dynamical symmetry restored and deconfinement occurred. It has been argued in the Ref. [42] that the appearance of the parameter η is because of the factor $(N_f - 2)$ in Eq. (4).

With a particular choice of the flavor-dependent model Eq. (4), the dynamical quark

mass function is merely a constant and the the dressed quark propagator takes into a very simple form [52]:

$$S^{-1}(p) = i\gamma \cdot p + M_f . \quad (5)$$

It is because the wave function renormalization trivially tends to unity in this case, and the quark mass function M become momentum independent:

$$M_f = m_f + \frac{\alpha_{\text{eff}}\alpha_{N_f}^{N_c}}{2} \int^{\Lambda} \frac{d^4k}{(2\pi)^4} \text{Tr}[S_f(k)] . \quad (6)$$

Where M_f is the dynamical mass and $\alpha_{N_f}^{N_c} = \sqrt{1 - \frac{(N_f-2)}{N_f^c}} \left(N_c - \frac{1}{N_c}\right)$. After simplifying Eq. (6), we have

$$M_f = m_f + 2\alpha_{\text{eff}}\alpha_{N_f}^{N_c} \int \frac{d^4k}{(2\pi)^4} \frac{M}{k^2 + M^2} . \quad (7)$$

The quark-antiquark condensate which serves as an order parameter for the dynamical chiral symmetry breaking in this truncation, can be written as

$$-\langle \bar{q}q \rangle = \frac{M_f - m_f}{2\alpha_{\text{eff}}} . \quad (8)$$

Using $d^4k = (1/2)k^2 dk^2 \sin^2 \theta d\theta \sin \phi d\phi d\psi$, performing the trivial integration's and using the variable $s = k^2$ in Eq. (7), we have

$$M_f = m_f + \frac{\alpha_{\text{eff}}\alpha_{N_f}^{N_c}}{8\pi^2} \int_0^{\infty} ds \frac{s}{s + M_f^2} . \quad (9)$$

The above integral in Eq. (9) is divergent and we need to regularize it. In the present scenario we use the Schwinger proper-time regularization procedure [3]. In this procedure, we take the exponent integrand's denominator and then introduce an additional infrared cutoff, in addition to the conventional ultraviolet that is normally used in NJL model Studies. Accordingly, the confinement is implemented through an infrared cut-off [53]. The significance of adopting the mentioned regularization procedure is, the quadratic and logarithmic divergences remove and the axial-vector Ward-Takahashi identity [54, 55] is satisfied. From Eq. (9), the integrand's denominator reduced to:

$$\begin{aligned} \frac{1}{s + M_f^2} &= \int_0^{\infty} d\tau e^{-\tau(s+M_f^2)} \rightarrow \int_{\tau_{uv}^2}^{\tau_{ir}^2} d\tau e^{-\tau(s+M_f^2)} \\ &= \frac{e^{-\tau_{uv}^2(s+M_f^2)} - e^{-\tau_{ir}^2(s+M_f^2)}}{s + M_f^2} . \end{aligned} \quad (10)$$

Here, $\tau_{uv} = \Lambda_{uv}^{-1}$ is an ultra-violet regulator, which plays the dynamical role and sets the scale for all dimensional quantities. The $\tau_{ir} = \Lambda_{ir}^{-1}$ stands for the infrared regulator whose non zero value implements confinement by ensuring the absence of quarks production thresholds [56]. Hence τ_{ir} referred to as the confinement scale [44]. From Eq. (10), it is now clear that the location of the original pole is at $s = -M^2$, which is canceled by the numerator. Thus the propagator is free from real as well as the

complex poles, which is consistent with the definition of confinement i.e., “an excitation described by a pole-less propagator would never reach its mass-shell” [53].

After integration over ‘s’, the gap equation Eq. (9) is reduced to:

$$M_f = m_f + \frac{M_f^3 \alpha_{\text{eff}} \alpha_{N_f}^{N_c}}{8\pi^2} \Gamma(-1, \tau_{uv} M_f^2, \tau_{ir} M_f^2), \quad (11)$$

where

$$\Gamma(a, y_1, y_2) = \Gamma(a, y_1) - \Gamma(a, y_2) \quad (12)$$

with $\Gamma(a, y) = \int_y^\infty t^{a-1} e^{-t} dt$, is the incomplete Gamma function. The above equation Eq. (11), is the gap equation in vacuum which is regularized in the Schwinger proper time regularization scheme with two regulators. The confinement in this model can be triggered from the confining length scale [44, 18, 42]:

$$\tilde{\tau}_{ir} = \tau_{ir} \frac{M}{M_f}, \quad (13)$$

where $M = M(3, 2)$ is the dynamical mass for fixed $N_c = 3$, $N_c = 2$. Here $M_f = M(N_c, N_f)$ is the generalized color N_c and flavor N_f dependent dynamical mass. As, the τ_{ir} is introduced in the model to mimic confinement by ensuring the absence of quarks production thresholds, so in the presence of N_f and N_c , it is required to vary slightly with both N_f and N_c . Thus the entanglement between dynamical chiral symmetry breaking and confinement is expressed through an explicit N_f and N_c -dependent regulator i.e., $\tilde{\tau}_{ir} = \tau_{ir}(N_c, N_f)$, in the infrared. For chiral quarks (i.e., $m_f = 0$), the confining scale $\tilde{\tau}_{ir}$ diverges at the chiral symmetry restoration region. Next we discuss the general formalism of the gap equation and the Schwinger pair production rate in the in the presence of electric field and in the presence of electric field eE and for higher N_f and N_c .

3. Gap equation and Schwinger pair production rate in the presence of electric field

In this section, we discuss the gap equation in the presence of a uniform and homogeneous pure electric field eE . In QCD Lagrangian, the interaction with pure electric field A_μ^{ext} embedded in the covariant derivative,

$$D_\mu = \partial_\mu - iQ_f A_\mu^{\text{ext}}, \quad (14)$$

with $Q_f = (q_u = +2/3, q_d = -1/3)e$ is refers to the electric charges of u and d -quark, respectively. We choose the symmetric gauge vector potential $A_\mu^{\text{ext}} = -\delta_{\mu 0} x_3 E$, to obtain the resulting electric field along the z -axis. The gap equation in the presence of pure electric field continues to form Eq. (6), where $S_f(k)$ is now dressed with electric field eE , that is, $S_f(k) \rightarrow \tilde{S}_f(k)$ [3, 11, 13, 15, 57], and is given as

$$\tilde{S}_f(k) = \int_0^\infty d\tau e^{-\tau \left(M_f^2 + (k_4^2 + k_3^2) \frac{\tan(|Q_f E| \tau)}{|Q_f E| \tau} + k_1^2 + k_2^2 \right)}$$

$$\begin{aligned} & \times \left[M_f + i\gamma^4 \left(k_4 + \tan(|Q_f E \tau|) \right) k_3 - \gamma^3 (k_3 + \tan(|Q_f E \tau|) k_4) - \left(\gamma^2 k_2 - \gamma^1 k_1 \right) \right. \\ & \left. \times \left(1 + \tan(|Q_f E \tau|) \gamma^4 \gamma^3 \right) \right]. \end{aligned} \quad (15)$$

Where γ 's are the Dirac gamma matrices. Taking the trace “Tr” of the of the propagator Eq. (15), inserting it in Eq. (6) and after carrying out the the integration over k 's, the gap equation in the electric field eE and with the flavor-dependent contact interaction model of quark [42] is given by

$$M_f = m_f + \frac{\alpha_{\text{eff}} \alpha_{N_f}^{N_c}}{8\pi^2} \sum_f \int_0^\infty \frac{d\tau}{\tau^2} M_f e^{-\tau M_f^2} \left[\frac{|Q_f E|}{\tan(|Q_f E \tau|)} \right]. \quad (16)$$

Next, we separate the vacuum and electric field dependent part by using the vacuum subtraction scheme[11, 13], as given by

$$\begin{aligned} M_f &= m_f + \frac{\alpha_{\text{eff}} \alpha_{N_f}^{N_c}}{8\pi^2} \sum_f \int_0^\infty \frac{d\tau}{\tau^2} M_f e^{-\tau M_f^2} \\ &+ \frac{\alpha_{\text{eff}} \alpha_{N_f}^{N_c}}{8\pi^2} \sum_f \int_0^\infty \frac{d\tau}{\tau^2} M_f e^{-\tau M_f^2} \left[\frac{|Q_f E| \tau}{\tan(|Q_f E \tau|)} - 1 \right]. \end{aligned} \quad (17)$$

The vacuum integral can be regularized with the two regulators as in Eq. (11), and thus the Eq. (17) can be reduced to:

$$\begin{aligned} M_f &= m_f + \frac{M_f^3 \alpha_{\text{eff}} \alpha_{N_f}^{N_c}}{8\pi^2} \Gamma(-1, \tau_{uv}^2 M_f^2, \tau_{ir}^2 M_f^2) \\ &+ \frac{\alpha_{\text{eff}} \alpha_{N_f}^{N_c}}{8\pi^2} \sum_f \int_0^\infty \frac{d\tau}{\tau^2} M_f e^{-\tau M_f^2} \left[\frac{|Q_f E| \tau}{\tan(|Q_f E \tau|)} - 1 \right]. \end{aligned} \quad (18)$$

The Eq. (18) can also be written as

$$\begin{aligned} \frac{M_f - m_f}{\alpha_{\text{eff}}} &= \frac{M_f^3 \alpha_{N_f}^{N_c}}{8\pi^2} \Gamma(-1, \tau_{uv}^2 M_f^2, \tau_{ir}^2 M_f^2) \\ &+ \frac{\alpha_{N_f}^{N_c}}{8\pi^2} \sum_f \int_0^\infty \frac{d\tau}{\tau^2} M_f e^{-\tau M_f^2} \left[\frac{|Q_f E| \tau}{\tan(|Q_f E \tau|)} - 1 \right]. \end{aligned} \quad (19)$$

As we have already regularized the integral in Eq. (18), using the vacuum subtraction scheme but we still have poles associated with the tangent term in the denominator of our gap equation when $|Q_f E| \tau = n\pi$ with $n = 1, 2, 3, \dots$. Upon taking the principle value (real value) of the integral [11], given in Eq. (19), we have

$$\int_0^\infty \frac{d\tau}{\tau^2} e^{-\tau M_f^2} \left(\frac{|Q_f E| \tau}{\tan(|Q_f E \tau|)} - 1 \right) = |Q_f E| \text{Re} J(i M_f^2 / 2 |Q_f E|), \quad (20)$$

with

$$J(\zeta) = 2i \left[\left(\zeta - \frac{1}{2} \right) \log \zeta - \zeta - \log \Gamma(\zeta) + \frac{1}{2} \log 2\pi \right]. \quad (21)$$

The effective potential Ω , can be obtained by integrating the Eq. (19) over dynamical mass M_f :

$$\Omega = \frac{(M_f - m_f)^2}{2\alpha_{\text{eff}}} - \frac{\alpha_{N_f}^{N_c} M_f^4}{32\pi^2} \left[\frac{e^{-\tau M_f^2}}{\tau_{uv}^4} - \frac{e^{-\tau M_f^2}}{\tau_{ir}^4} - M_f^4 \Gamma(-1, \tau_{uv}^2 M_f^2, \tau_{ir}^2 M_f^2) \right] - \frac{\alpha_{N_f}^{N_c}}{16\pi^2} \sum_f \int_0^\infty \frac{d\tau}{\tau^3} M_f e^{-\tau M_f^2} \left[\frac{|Q_f E| \tau}{\tan(|Q_f E| \tau)} - 1 \right]. \quad (22)$$

We noted that there are infinite poles in the effective potential Ω too which are due to the contribution of the Schwinger pair production in the presence of the tangent (electric field-related) term. These poles yields the effective potential to be complex with its imaginary part giving the Schwinger pair production rate [3, 16, 13, 14]. The third term in the Eq. (22) can be further simplified by using the following trigonometric relation:

$$\frac{\pi \tau}{\tan(\pi \tau)} - 1 = \sum_{n=1}^{\infty} \frac{2\tau^2}{\tau^2 - n^2}. \quad (23)$$

Using Eq. (23) in Eq. (22), we have

$$\Omega = \frac{(M_f - m_f)^2}{2\alpha_{\text{eff}}} - \frac{\alpha_{N_f}^{N_c} M_f^4}{32\pi^2} \left[\frac{e^{-\tau M_f^2}}{\tau_{uv}^4} - \frac{e^{-\tau M_f^2}}{\tau_{ir}^4} - M_f^4 \Gamma(-1, \tau_{uv}^2 M_f^2, \tau_{ir}^2 M_f^2) \right] - \frac{\alpha_{N_f}^{N_c}}{16\pi^2} \sum_f \int_0^\infty \frac{d\tau}{\tau^3} M_f e^{-\tau M_f^2} \sum_{n=1}^{\infty} \frac{2\tau^2}{\tau^2 - \frac{\pi^2 n^2}{(|Q_f E|)^2}}. \quad (24)$$

The Schwinger pair production rate Γ , corresponds to the imaginary part of the effective potential Eq. (24), and is thus, given by

$$\Gamma = -2\text{Im}\Omega = \sum_f \sum_{n=1}^{\infty} \frac{\alpha_{N_f}^{N_c} (|Q_f E|)^2 e^{-n\pi M_f^2/|Q_f E|}}{4\pi (n\pi)^2}, \quad (25)$$

which does not depend on the number of color N_c or the number of flavors N_f explicitly. However, since the dynamical quark mass M_f depends on both N_f and N_c as it is obvious from the gap equation Eq. (17), they will affect the quark-antiquark pair production rate Γ implicitly through M_f . The numerical solution of the gap equation and the Schwinger pair production rate will be discussed in the next section.

4. Numerical Results

In this section, we present the numerical results of the gap equation at zero electric field and in the presence of electric field for higher N_c and N_f . We use the following set of flavor-dependent contact interaction model parameters [42] i.e., $\tau_{ir} = (0.24 \text{ GeV})^{-1}$, $\tau_{uv} = (0.905 \text{ GeV})^{-1}$, and bare quark mass $m_u = m_d = 0.007 \text{ GeV}$. For fixed $N_c = 3$ and $N_f = 2$, we have obtained the dynamical mass $M_{u,d} = 0.367 \text{ GeV}$ and the condensate $-\langle \bar{q}q \rangle_{u,d}^{1/3} = 0.243 \text{ GeV}^3$. It should be noted that these parameters were fitted to reproduce the light mesons properties [49].

Next, we solve the gap equation Eq.(11) for various N_f and at fix $N_c = 3$ as shown

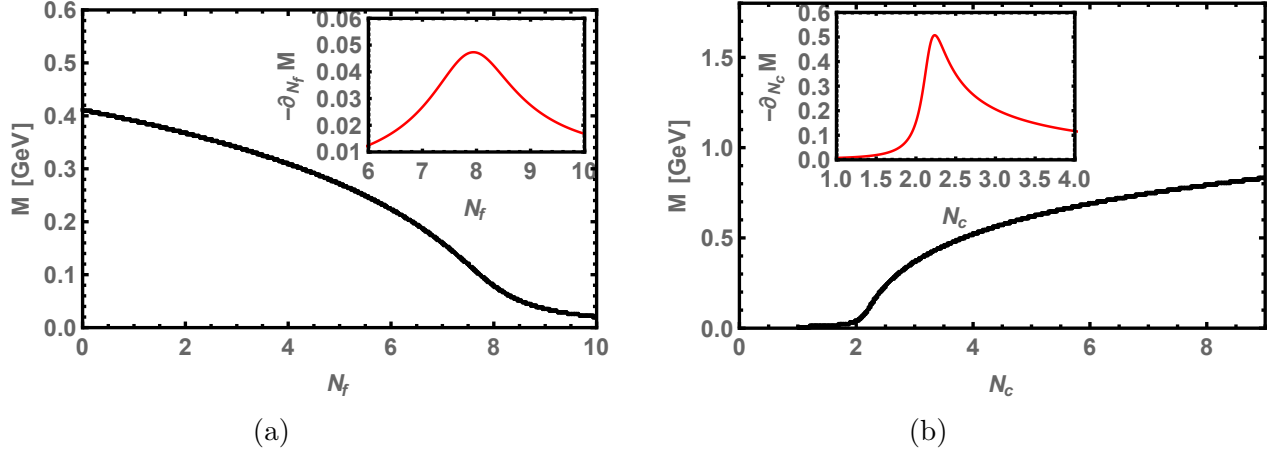


Figure 1: (a) Behavior of the dynamical quark mass M and its flavor-gradient $\partial_{N_f} M$ as a function of number of flavors N_f for fixed number of $N_c = 3$. The dynamical mass M decreases as we increase N_f and at some critical value $N_f^c = 8$, the dynamical chiral symmetry is restored.

(b) The behavior of the dynamical quark mass M and its color-gradient $\partial_{N_c} M$ as a function of number of colors N_c and for fixed $N_f = 2$. From the peak of the $\partial_{N_c} M$, it is clear that the dynamical chiral symmetry is broken above $N_c^c = 2.2$.

in the Fig. 1. The dynamical mass monotonically decreases as we increase the N_f as depicted in Fig. 1(a). The plot inside the Fig. 1(a), represents the flavor-gradient of the dynamical mass $\partial_{N_f} M_f$, whose peak is at $N_f^c \approx 8$, which is a critical number of flavors where near and above the dynamical chiral symmetry restored. In Fig. 1(b), we show the dynamical mass as a function of the number of colors N_c for fix $N_f = 2$. This plot represents that the dynamical chiral symmetry broken near or above some critical value of $N_c^c \approx 2.2$. The $N_c^c \approx 2.2$ is obtained from the peak of the color-gradient of the mass function $\partial_{N_c} M_f$. These findings are consistent with results obtained in [42, 43]. The inverse of the confining length scale $\tilde{\tau}_{ir}^{-1}$ and its flavor-gradient plotted for various N_f and for fixed $N_c = 3$ are plotted in Fig. 2(a). The confinement can be triggered from flavor-gradient $\partial_{N_f} \tilde{\tau}_{ir}^{-1}$, whose peak is at $N_f^c \approx 8$, and is approximated as a critical number of flavors above which the quark become unconfined. In Fig. 2(b), we show the inverse confining length scale $\tilde{\tau}_{ir}^{-1}$ as a function of the various number of colors N_c for fix $N_f = 2$. This plot represents that the confinement occurs near and above at some critical value of $N_c^c \approx 2.2$. The critical $N_c^c \approx 2.2$ for the confinement is obtained from the peak of the color gradient $\partial_{N_c} \tilde{\tau}_{ir}^{-1}$. Next, we solve the gap equation Eq. (17), in the presence of electric field eE and plotted the dynamical mass as a function of eE , for the various number of flavors N_f and for fix $N_c = 3$ as depicted in Fig. 3(a). The dynamical mass decreases as we increase the electric field eE as we expected. Upon increasing the N_f , the plateau of dynamical quark mass as a function of eE suppresses for larger values of N_f . There is no dynamical mass generation above $N_f^c = 8$, this is because both electric field eE and N_f restore the dynamical chiral symmetry and quarks

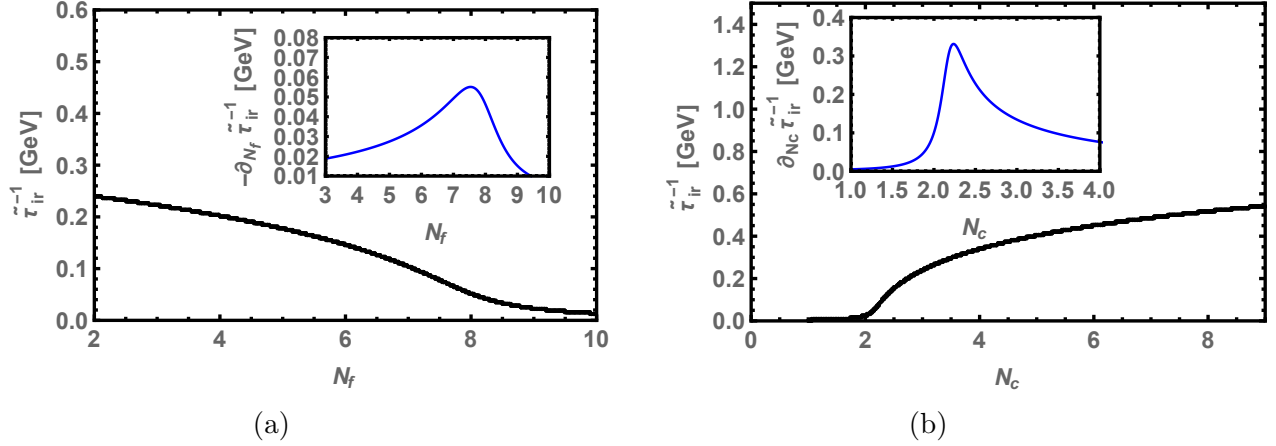


Figure 2: (a) Behavior of the inverse of confining length scale $\tilde{\tau}_{ir}^{-1}$ and its flavor-gradient $\partial_{N_f} \tilde{\tau}_{ir}^{-1}$ as a function of number of flavors N_f for fixed $N_c = 3$. (b) The behavior $\tilde{\tau}_{ir}^{-1}$ and its color-gradient $\partial_{N_c} \tilde{\tau}_{ir}^{-1}$ as a function of the number of colors N_c and for fixed $N_f = 2$.

becomes unconfined.

In Fig. 3(b), we plotted the dynamical quark mass as a function of electric field strength eE for various N_c and for fixed $N_f = 2$. The increasing N_c enhances the plateau of the dynamical mass as a function of eE . For $N_c \geq 4$, the mass plots show the discontinuities in the dynamical symmetry restoration region where the nature of smooth cross-over phase transition changes to the first order. This may be due to the strong competition that occurs between eE and N_c (i.e. strong electric field tends to restore the dynamical chiral symmetry whereas larger N_c enhance the dynamical chiral symmetry breaking).

The Schwinger pair production rate “ Γ ” Eq. (25), as a function of electric field strength eE , for various N_f and for fix $N_c = 3$ is shown in the Fig. 4(a). This figure clearly demonstrate that after some critical value eE_c , where near at and above the dynamical symmetry restored and the deconfinement occurred, the pair production rate “ Γ ” grows faster due to the weakening of the chiral condensates. In this situation, the QCD vacuum becomes more unstable and the pair of quark-antiquark becomes more likely to produces. Upon increasing the number of flavors N_f , the pair production rate grows faster and shifted towards the lower values of electric field eE . This is because, both the eE and N_f restore the dynamical chiral symmetry. Although, there is an unstable slow enhancement of pair production rate for small N_f but become stable and faster for higher values of N_f . In Fig. 4(b), we plotted the quark-antiquark pair production rate “ Γ ” as a function of eE for various N_c but at this time we fix the number of flavors $N_f = 2$. Upon increasing the number of colors N_c , the production rate grows slowly and higher values of eE are needed for a stable and faster production rate. This is because, N_c enhances the dynamical chiral symmetry breaking. For $N_c \geq 4$, the discontinuity occurs in the production rate near and above the chiral symmetry restoration and deconfinement region. This may be due to the strong competition

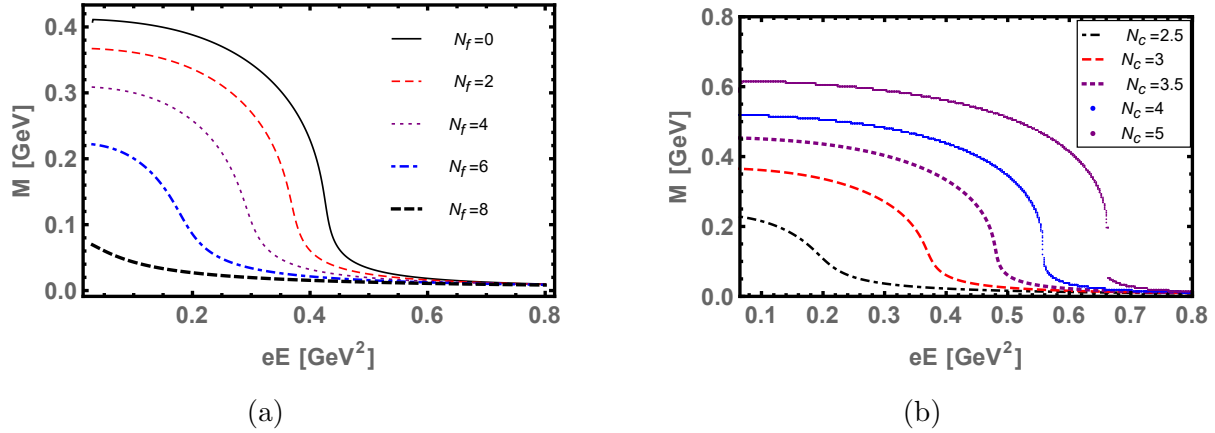


Figure 3: (??) The dynamical quark mass as a function of electric field strength eE , for various N_f and for fixed $N_c = 3$. The plateau of the dynamical mass suppresses as we increase N_f . (b) shows the behavior of the dynamical quark mass as a function of electric field strength eE for various N_c and for fixed $N_f = 2$. The increasing N_c enhances the plateau of the dynamical mass as a function of eE . For $N_c \geq 4$, the cross-over phase transition changes to the first order.

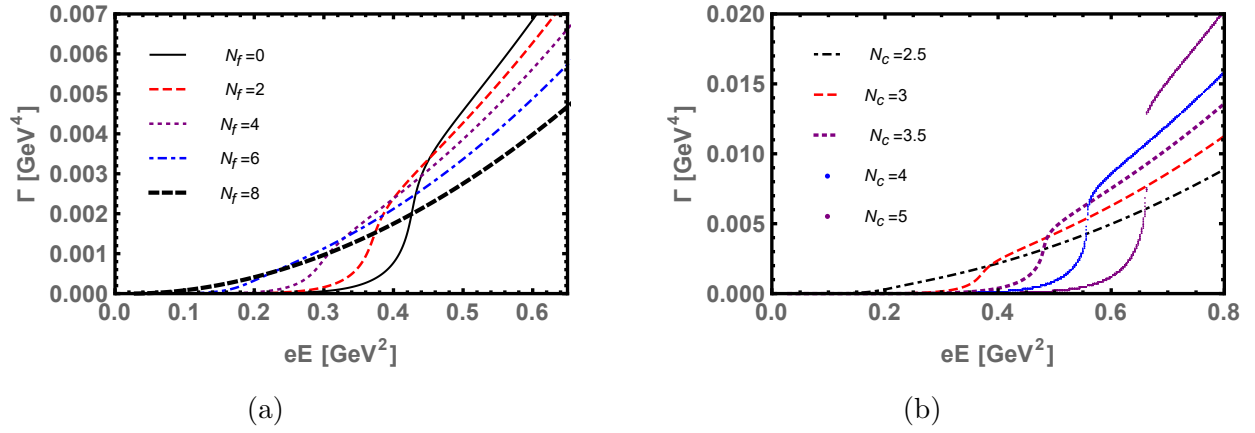


Figure 4: (a) The Schwinger pair production rate Γ as a function of electric field strength eE , for various N_f and for fixed $N_c = 3$. Upon increasing N_f , the pair production rate grows faster even at small values of eE . (b) The behavior of production rate Γ as a function of eE for various N_c at fixed $N_f = 2$. Upon increasing the number of colors N_c the production rate grows slowly and higher values of eE needed for quick and stable pair production rate.

between N_c and eE , i.e., on one hand, the strong electric field eE tends to restore the dynamical chiral symmetry whereas the N_c tends to break it. We then obtained the pseudo-critical electric field eE_c for the chiral symmetry breaking -restoration from the electric field-gradient $\partial_{eE} M_f$ as a function of eE for various N_f and at fixed $N_c = 3$, as depicted in Fig. 5(a). The peaks of the $\partial_{eE} M_f$ shift towards lower values of the electric field eE . In Fig. 5(b), we plotted the electric field gradient $\partial_{eE} M_f$ as a function of

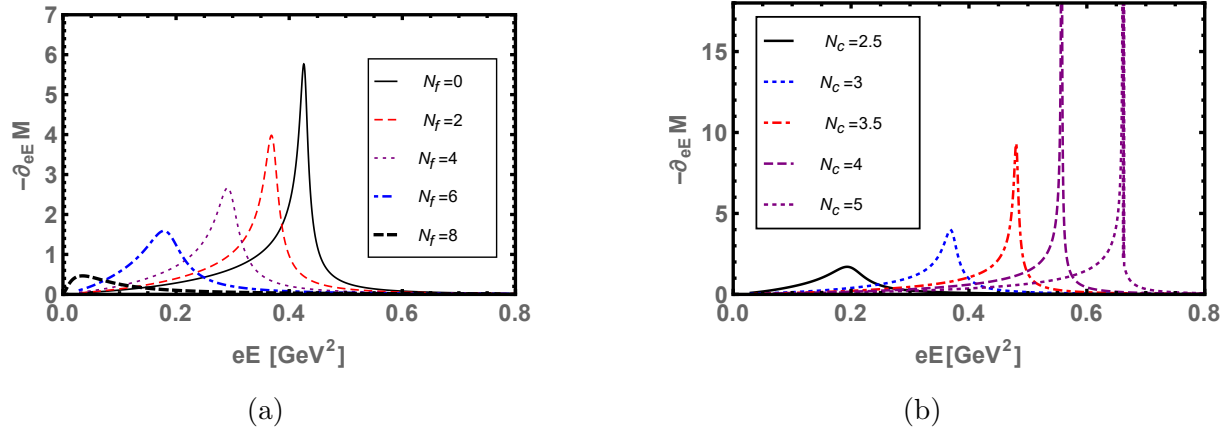


Figure 5: (a) The electric-gradient of the dynamical mass $\partial_{eE} M$ as a function N_f for fixed $N_c = 3$. The peaks shifted towards the lower values of electric field eE upon the increasing N_f . (b) The electric-gradient $\partial_{N_c} M$ as a function of N_c for fixed $N_f = 2$. The peak of the $\partial_{N_c} M$, shifts toward higher values of eE as N_c increases. For $N_c \geq 4$, the peaks in $\partial_{N_c} M$ diverges and dicontinuous.

eE for various N_c and at fixed $N_f = 2$. Upon increasing N_c , the peaks shift towards higher values of eE . We then obtained the pseudo-critical electric field eE_c for the chiral symmetry restoration/deconfinement different N_f , and draw a phase diagram in $N_f - eE$ plane a shown in the Fig. 6(a). The pseudo-critical electric field eE_c decreases as we increase N_f , the nature of the chiral phase transition is of smooth cross-over. In Fig. 6(b), we sketch the phase diagram in $N_c - eE_c$ plane, the critical eE_c grows upon increasing the number of colors N_c . The transition is of smooth cross-over until the critical endpoint ($N_{c,p} = 4, eE_{c,p} = 0.54 GeV^2$) where it suddenly changes to the first-order. The phase diagram also shows that the quark-antiquark pair production grows quickly after pseudo-critical electric field eE_c and how it varies with the flavors and colors. Our finding for $N_c = 3$ and $N_f = 2$, agrees well with the growth of the quark-antiquark production rate studied through another effective model of low energy QCD [31, 14]. In the next section, we discuss the summery and future perspectives of the this work.

5. Summery and Perspectives

In this work, we have studied the impact of pure electric field on the color-flavor chiral phase transitions and investigated the Schwinger quark-antiquark pair production rate Γ for the higher number of colors N_c and number flavors N_f . For this purpose, we implemented the Schwinger-Dyson formulation of QCD, with a gap equation kernel comprising a symmetry-preserving vector-vector flavor-dependent contact interaction model of quarks in a rainbow-ladder truncation. Subsequently, we adopted the well-known Schwinger proper-time regularization procedure. The outcome of this study is presented as follows:

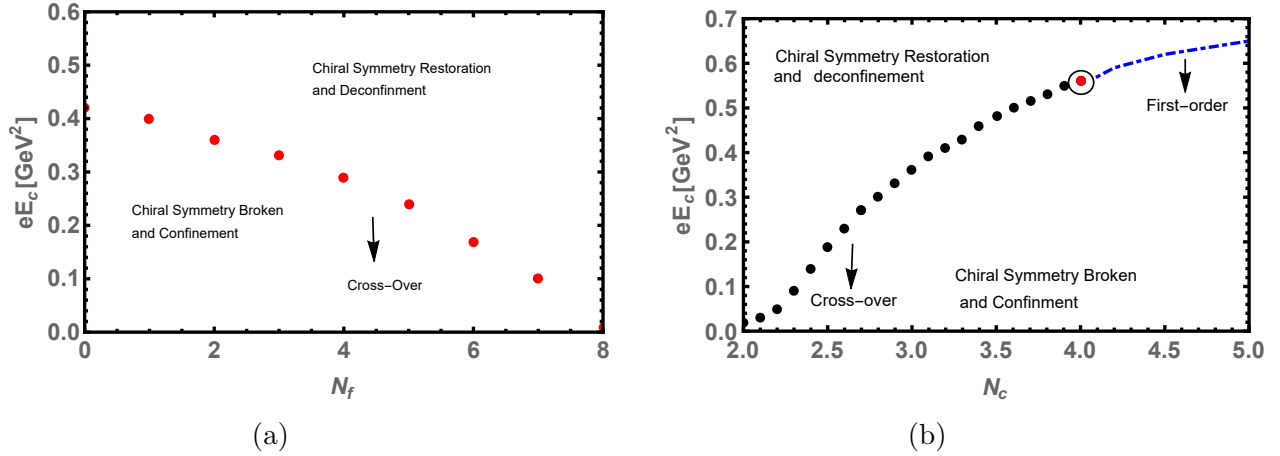


Figure 6: (a) The phase diagram $N_f - eE_c$ plane for the dynamical chiral symmetry breaking/restoration or confinement-deconfinement transition. The pseudo-critical eE_c decreases upon increasing the number of light quark flavors N_f . (b) The phase diagram in $N_c - eE_c$ plane; here the critical eE increase upon increasing the number of color N_c . The transition is of smooth cross-over until the critical endpoint $(N_{c,p}^c, eE_{c,p})$ where it suddenly changes to the first-order.

First, we reproduced the results of dynamical chiral symmetry restoration for large N_f with fixed $N_f = 3$, where we evaluated the critical number of flavors $N_f^c \approx 8$. Further, we explore the dynamical symmetry breaking for a higher number of colors N_c but kept $N_f = 2$ and found the critical number of colors $N_c^c \approx 2.2$. Second, we consider the influence of the pure electric field eE , where we have explored the dynamical chiral symmetry restoration and deconfinement for various numbers of flavors N_f and colors N_c . The plateau of the mass as a function of the electric field is noted to suppress upon increasing the number of flavors. Whereas upon increasing the number of colors, the dynamical mass as a function of eE enhances and at some $N_c \geq 4$, we found the discontinuity in the chiral symmetry restoration region. Next, We obtained the Schwinger pair production (quark-antiquark) rate Γ as a function of the pure electric field eE for various N_f and N_c . For fixed $N_c = 3$, and upon varying the N_f , we found that quark-antiquark production rate Γ grows quickly when we cross a pseudo-critical electric field eE_c . As a result, the pair production rate tends to initiate at lower values of eE for larger values of N_f . Hence, the pseudo-critical electric field eE_c reduced in magnitude upon increasing the number of flavors N_f . This is because both N_f and eE restored the dynamical chiral symmetry. While for fixed $N_f = 2$ and upon increasing N_c , the Schwinger pair production tends to initiate at larger values of eE for higher values of N_c . It is interesting to note that for $N \geq 4$, the discontinuity occurred in the production rate in the region where the chiral symmetry is restored. This may be due to the strong competition that occurred between eE and N_c . Thus, the pseudo-critical eE_c enhances as the number of colors N_c increases. The transition is of smooth cross-over until the critical endpoint $(N_{c,p}^c, eE_{c,p} = 0.54 \text{ GeV}^2)$, where it suddenly

changes to the first order. Our finding for $N_c = 3$ and $N_f = 2$ agrees well with the behaviour of the pair production rate studied through other effective models of low energy QCD. Qualitatively and quantitatively, the predictions of the presented flavor-dependent contact interaction model for fixed $N_c=3$ and $N_f = 2$ agree well with results obtained from other effective QCD models. Soon, we plan to extend this work to study the Schwinger pair production rate in hot and dense matter QCD in the presence of background fields. We are also interested in extending this work to study the properties of light hadrons in the background fields etc.

6. Acknowledgments

We acknowledge A. Bashir and A. Raya for their guidance and valuable suggestions in the process of completion of this work. We also thank to the colleagues of the Institute of Physics, Gomal University (Pakistan).

References

- [1] Sauter F 1931 *Z. Phys.* **69** 742–764
- [2] Heisenberg W and Euler H 1936 *Z. Phys.* **98** 714–732 (*Preprint* physics/0605038)
- [3] Schwinger J S 1951 *Phys. Rev.* **82** 664–679
- [4] Yildiz A and Cox P H 1980 *Phys. Rev. D* **21** 1095
- [5] Cox P H and Yildiz A 1985 *Phys. Rev. D* **32** 819–820
- [6] Suganuma H and Tatsumi T 1991 *Annals Phys.* **208** 470–508
- [7] Suganuma H and Tatsumi T 1993 *Prog. Theor. Phys.* **90** 379–404
- [8] Tanji N 2009 *Annals Phys.* **324** 1691–1736 (*Preprint* 0810.4429)
- [9] Klevansky S P and Lemmer R H 1988 *Phys. Rev.* **D38** 3559–3565
- [10] Klimenko K G 1992 *Theor. Math. Phys.* **90** 1–6 [*Teor. Mat. Fiz.*90,3(1992)]
- [11] Klevansky S P 1992 *Rev. Mod. Phys.* **64** 649–708
- [12] Babansky A Yu, Gorbar E V and Shchepanyuk G V 1998 *Phys. Lett.* **B419** 272–278 (*Preprint* hep-th/9705218)
- [13] Cao G and Huang X G 2016 *Phys. Rev. D* **93** 016007 (*Preprint* 1510.05125)
- [14] Tavares W R and Avancini S S 2018 *Phys. Rev. D* **97** 094001 (*Preprint* 1801.10566)
- [15] Wang L and Cao G 2018 *Phys. Rev.* **D97** 034014 (*Preprint* 1712.09780)
- [16] Ruggieri M and Peng G X 2016 *Phys. Rev.* **D93** 094021 (*Preprint* 1602.08994)
- [17] Tavares W R, Farias R L S and Avancini S S 2020 *Phys. Rev. D* **101** 016017 (*Preprint* 1912.00305)
- [18] Ahmad A 2021 *Chin. Phys. C* **45** 073109 (*Preprint* 2009.09482)
- [19] Bzdak A and Skokov V 2012 *Phys. Lett.* **B710** 171–174 (*Preprint* 1111.1949)
- [20] Deng W T and Huang X G 2012 *Phys. Rev. C* **85** 044907 (*Preprint* 1201.5108)
- [21] Bloczynski J, Huang X G, Zhang X and Liao J 2013 *Phys. Lett.* **B718** 1529–1535 (*Preprint* 1209.6594)
- [22] Bloczynski J, Huang X G, Zhang X and Liao J 2015 *Nucl. Phys.* **A939** 85–100 (*Preprint* 1311.5451)
- [23] Hirono Y, Hongo M and Hirano T 2014 *Phys. Rev. C* **90** 021903 (*Preprint* 1211.1114)
- [24] Voronyuk V, Toneev V D, Voloshin S A and Cassing W 2014 *Phys. Rev. C* **90** 064903 (*Preprint* 1410.1402)
- [25] Deng W T and Huang X G 2015 *Phys. Lett. B* **742** 296–302 (*Preprint* 1411.2733)
- [26] Huang X G and Liao J 2013 *Phys. Rev. Lett.* **110** 232302 (*Preprint* 1303.7192)
- [27] Jiang Y, Huang X G and Liao J 2015 *Phys. Rev.* **D91** 045001 (*Preprint* 1409.6395)

- [28] Karpenko I and Becattini F 2017 *Eur. Phys. J.* **C77** 213 (*Preprint* 1610.04717)
- [29] Xia X L, Li H, Tang Z B and Wang Q 2018 *Phys. Rev.* **C98** 024905 (*Preprint* 1803.00867)
- [30] Wei D X, Deng W T and Huang X G 2019 *Phys. Rev.* **C99** 014905 (*Preprint* 1810.00151)
- [31] Cao G and Zhuang P 2015 *Phys. Rev. D* **92** 105030 (*Preprint* 1505.05307)
- [32] Appelquist T *et al.* (LSD) 2014 *Phys. Rev. D* **90** 114502 (*Preprint* 1405.4752)
- [33] Hayakawa M, Ishikawa K I, Osaki Y, Takeda S, Uno S and Yamada N 2011 *Phys. Rev. D* **83** 074509 (*Preprint* 1011.2577)
- [34] Cheng A, Hasenfratz A, Petropoulos G and Schaich D 2013 *JHEP* **07** 061 (*Preprint* 1301.1355)
- [35] Hasenfratz A and Schaich D 2018 *JHEP* **02** 132 (*Preprint* 1610.10004)
- [36] Appelquist T *et al.* (Lattice Strong Dynamics) 2019 *Phys. Rev. D* **99** 014509 (*Preprint* 1807.08411)
- [37] Bashir A, Raya A and Rodriguez-Quintero J 2013 *Physical Review D* **88** 054003
- [38] Appelquist T, Cohen A G and Schmaltz M 1999 *Phys. Rev. D* **60** 045003 (*Preprint* hep-th/9901109)
- [39] Hopfer M, Fischer C S and Alkofer R 2014 *JHEP* **11** 035 (*Preprint* 1405.7031)
- [40] Doff A and Natale A A 2016 *Phys. Rev. D* **94** 076005 (*Preprint* 1610.02564)
- [41] Binosi D, Roberts C D and Rodriguez-Quintero J 2017 *Phys. Rev. D* **95** 114009 (*Preprint* 1611.03523)
- [42] Ahmad A, Bashir A, Bedolla M A and Cobos-Martínez J J 2021 *J. Phys. G* **48** 075002 (*Preprint* 2008.03847)
- [43] Ahmad A and Murad A 2022 *Chin. Phys. C* **46** 083109 (*Preprint* 2201.09980)
- [44] Ahmad A and Raya A 2016 *J. Phys.* **G43** 065002 (*Preprint* 1602.06448)
- [45] Marquez F, Ahmad A, Buballa M and Raya A 2015 *Phys. Lett.* **B747** 529–535 (*Preprint* 1504.06730)
- [46] Langfeld K, Kettner C and Reinhardt H 1996 *Nucl. Phys. A* **608** 331–355 (*Preprint* hep-ph/9603264)
- [47] Cornwall J M 1982 *Phys. Rev. D* **26** 1453
- [48] Aguilar A C, Binosi D and Papavassiliou J 2016 *Front. Phys. (Beijing)* **11** 111203 (*Preprint* 1511.08361)
- [49] Gutierrez-Guerrero L X, Bashir A, Cloet I C and Roberts C D 2010 *Phys. Rev.* **C81** 065202 (*Preprint* 1002.1968)
- [50] Kohyama H 2016 (*Preprint* 1602.09056)
- [51] Boucaud P, Leroy J P, Yaouanc A L, Micheli J, Pene O and Rodriguez-Quintero J 2012 *Few Body Syst.* **53** 387–436 (*Preprint* 1109.1936)
- [52] Ahmad A, Ayala A, Bashir A, Gutiérrez E and Raya A 2015 *J. Phys. Conf. Ser.* **651** 012018
- [53] Ebert D, Feldmann T and Reinhardt H 1996 *Phys. Lett.* **B388** 154–160 (*Preprint* hep-ph/9608223)
- [54] Ward J C 1950 *Phys. Rev.* **78** 182
- [55] Takahashi Y 1957 *Nuovo Cim.* **6** 371
- [56] Roberts C D, Bhagwat M S, Holl A and Wright S V 2007 *Eur. Phys. J. ST* **140** 53–116 (*Preprint* 0802.0217)
- [57] Cao G 2021 *Eur. Phys. J. A* **57** 264 (*Preprint* 2103.00456)